A MUSE survey of the dense halo gas in z~3 galaxies near optically-thick absorbers

Abstract

This is the second data release (DR2) of MUSE cubes obtained in quasar fields at z~3-4.5 as part of the Large Programme ID 197.A-0384, aimed at studying the distribution of gas around galaxies. For each of the 28 quasar fields in the survey we release the final coadded data cubes reduced using the CubEx software (Cantlaupo et al. 2019) along with the associated white-light images.

Overview of Observations

Observations for this large programme have been obtained between period 96 and period 103 using the MUSE instrument in wide-field mode with extended wavelength coverage, encompassing a region of approximately 1x1 arcmin^2 with the targeted quasar close to the centre of the field of view. Observations collected exclusively as part of the Large Programme ID 197.A-0384 have been acquired in a series of 5 observing blocks, where each observing block was composed of ~3x960s exposures, totaling ~4 hours of observation on source. Four objects (J012403+004432, J111113-080401, J120917+113830, J193957-100241) include also archival data, collected as part of the programmes ID 094.A-0585, 094.A-0131, 095.A-0200, 096.A-0222. For three of these objects (all but J012403+004432), the archival data have been collected in nominal wavelength mode and combined with data in extended mode collected as part of this large programme. In this data release, we also include the CubEx reductions for five quasars taken solely from archival data, including from the MUSEQuBES survey (Muzahid et al. 2020). These systems are J095852+120245, J102009+104002, J142438+225600, J162116-004251, J200324-325145 and data was observed as part of the programmes 094.A-0280, 095.A-0200, 099.A-0159, 097.A-0089, 094.A-0131.

Release Content

Data for the sources listed in the following table[1] are released.

The table lists: the reference name of the quasar; the common name in the NASA/IPAC Extragalactic Database (NED); the right ascension and declination of the quasar near the centre of the field (J2000), note that the RA and Dec of the associated fits files report the centre coordinates of each field; the quasar r-band magnitude with its associated uncertainty; the quasar redshift derived from rest-frame UV lines with its associated uncertainty; the number of known strong absorption line systems; the total on-source exposure time of MUSE observations; the programme number under which observations have been collected; the resulting image quality in the reconstructed r-band from MUSE data; the limiting flux (1σ pixel rms) measured at 5500A and the corresponding AB magnitude (2σ) for a 0.7 arcsec aperture. For further details on the listed quantities see Lofthouse et al. 2020, doi:10.1093/mnras/stz3066.

[1] This table is extracted from the publication Lofthouse et al. 2020 in Monthly Notices of the Royal Astronomical Society, Volume 491, Issue 2, January 2020, Pages 2057–2074, https://doi.org/10.1093/mnras/stz3066

Table 1. Summary of the sample properties and MUSE observations. The table lists: the reference name of the quasar; the common name in the NASA/IPAC Extragalactic Database (NED); the right ascension and declination of the quasar at the centre of the field (J2000); the quasar r band magnitude with its associated uncertainty; the quasar redshift derived from rest-frame UV lines with its associated uncertainty; the number of known strong absorption line systems with $N_{\rm HI} \gtrsim 10^{17}$ cm^{-2}; the total on-source exposure time of MUSE observations; the programme number under which observations have been collected; the resulting image quality in the reconstructed r band from MUSE data; the limiting flux (1σ pixel rms) measured at 5500 Å and the corresponding AB magnitude (2σ) for a 0.7 arcsec aperture.

Name	Common Name	R.A. (hh:mm:ss)	Dec. (dd:mm:ss)	$m_{\rm r}$ (mag)	$z_{\rm qso,uv}$	$N_{\rm lls}$	$t_{\rm exp}^{\rm MUSE}$ (hours)	PID	I.Q. (arcsec)	$F_{\rm rms}/m_{\rm ap}$ (10^{-20}erg s^{-1} cm^{-2} Å^{-1}/mag)
J010619.24+004823.3[a]	SDSS J010619.24+004823.3	01:06:19.24	+00:48:23.31	19.10(0.01)	4.4402(0.0002)	2	4.02	197.A–0384	0.67	1.84/26.25
J012403.77+004432.7[a]	QSO J0124+0044	01:24:03.77	+00:44:32.76	17.95(0.01)	3.8359(0.0003)	2	4.38	197.A–0384,096.A–0222	0.73	1.99/26.16
J013340.31+040059.7[a]	KODIAQ J013340+040059	01:33:40.31	+04:00:59.77	18.45(0.01)	4.1709(0.0002)	3	4.02	197.A–0384	0.63	1.86/26.24
J013724.36–422417.3[c]	BRI J0137–4224	01:37:24.36	–42:24:17.30	18.46(0.05)	3.975(0.012)[d]	2	4.82	197.A–0384	0.68	1.41/26.54
J015741.56–010629.6[a]	SDSS J015741.56–010629.6	01:57:41.56	–01:06:29.66	18.30(0.01)	3.5645(0.0001)	2	4.02	197.A–0384	0.77	1.78/26.29
J020944.61+051713.6[a]	SDSS J020944.61+051713.6	02:09:44.61	+05:17:13.66	18.44(0.01)	4.1846(0.0006)	3	4.55	197.A–0384	0.57	1.58/26.41
J024401.84–013403.7[a]	BRI 0241–0146	02:44:01.84	–01:34:03.78	18.18(0.01)	4.044(0.012)[d]	2	4.02	197.A–0384	0.67	1.62/26.39
J033413.42–161205.4[b]	BR 0331–1622	03:34:13.42	–16:12:05.36	18.63(0.01)	4.380(0.013)[d]	2	4.02	197.A–0384	0.67	1.66/26.36
J033900.98–013317.7[c]	PKS 0336–017	03:39:00.98	–01:33:17.70	19.17(0.05)	3.204(0.009)[d]	2	4.02	197.A–0384	0.62	1.61/26.40
J094932.26+033531.7[a]	SDSS J094932.26+033531.7	09:49:32.26	+03:35:31.78	18.03(0.01)	4.1072(0.0004)	2	4.02	197.A–0384	0.69	1.82/26.26
J095852.19+120245.0[a]	Q0956+122	09:58:52.19	+12:02:45.04	17.47(0.01)	3.2746(0.0003)	2	4.10	094.A–0280	0.60	2.95/25.73
J102009.99+104002.7[a]	PKS 1017+109	10:20:09.99	+10:40:02.73	17.72(0.01)	3.1528(0.0003)	1	4.40	096.A–0937	0.69	2.07/26.12
J111008.61+024458.0[a]	SDSS J111008.61+024458.0	11:10:08.61	+02:44:58.07	18.28(0.01)	4.1582(0.0003)	2	4.02	197.A–0384	0.72	1.97/26.17
J111113.79–080402.0[b]	BRI 1108–0747	11:11:13.79	–08:04:02.00	18.49(0.01)	3.930(0.012)[d]	3	4.41	197.A–0384,095.A–0200	0.70	2.26/26.02
J120917.93+113830.3[a]	[HB89] 1206+119	12:09:17.93	+11:38:30.34	17.45(0.01)	3.0836(0.0001)	2	3.96	197.A–0384,094.A–0585	0.66	1.88/26.22
J123055.57–113909.3[c]	QSO J1230-1139	12:30:55.57	–11:39:09.30	19.84(0.05)	3.557(0.012)[d]	1	4.02	197.A–0384	0.66	1.75/26.30
J124957.23–015928.8[a]	SDSS J124957.23–015928.8	12:49:57.23	–01:59:28.80	17.78(0.01)	3.6337(0.0003)	1	4.02	197.A–0384	0.65	2.10/26.11
J133254.51+005250.6[a]	SDSS J133254.51+005250.6	13:32:54.51	+00:52:50.63	18.35(0.01)	3.5071(0.0001)	1	4.02	197.A–0384	0.65	1.62/26.38
J142438.10+225600.7[a]	QSO B1422+231	14:24:38.10	+22:56:00.71	15.17(0.01)	3.634(0.012)[d]	1	4.00	095.A–0200,099.A–0159	0.83	2.29/26.01
J162116.92–004250.8[a]	QSO J1621-0042	16:21:16.92	–00:42:50.86	17.28(0.01)	3.7100(0.0002)	1	9.76	095.A–0200,097.A–0089	0.65	1.92/26.20
J193957.25–100241.5[c]	PKS 1937–101	19:39:57.25	–10:02:41.50	16.61(0.05)	3.787(-)[e]	1	4.61	197.A–0384,094.A–0131	0.80	2.00/26.16
J200324.14–325144.8[c]	QSO B2000-330	20:03:24.14	–32:51:44.80	17.38(0.05)	3.785(0.011)[d]	3	10.00	094.A–0131	0.74	1.45/26.51
J205344.72–354655.2[c]	[WHO91] 2050–359	20:53:44.72	–35:46:55.20	18.41(0.05)	3.490(-)[e]	2	4.02	197.A–0384	0.66	2.16/26.07
J221527.29–161133.0[b]	BR 2212–1626	22:15:27.29	–16:11:33.00	18.13(0.01)	4.000(0.013)[d]	2	4.02	197.A–0384	0.68	2.26/26.02
J230301.45–093930.7[a]	SDSS J230301.45–093930.6	23:03:01.45	–09:39:30.72	17.68(0.01)	3.4774(0.0003)	1	4.02	197.A–0384	0.69	1.75/26.30
J231543.56+145606.4[a]	SDSS J231543.56+145606.4	23:15:43.56	+14:56:06.41	18.54(0.01)	3.3971(0.0004)	2	4.28	197.A–0384	0.73	1.77/26.29
J233446.40–090812.2[a]	FBQS J2334–0908	23:34:46.40	–09:08:12.24	18.03(0.01)	3.3261(0.0005)	2	4.02	197.A–0384	0.74	1.66/26.36
J234913.75–371259.2[b]	BR J2349–3712	23:49:13.75	–37:12:59.25	19.15(0.02)	4.240(0.012)[d]	2	4.28	197.A–0384	0.71	1.56/26.43

[a] Entries related to the quasar (R.A., Dec., $m_{\rm r}$ and $z_{\rm qso,uv}$) are, unless otherwise noted, from SDSS (Abolfathi et al. 2017). [b] Quasar photometry (R.A., Dec., $m_{\rm r}$) is from the ATLAS survey (Shanks et al. 2015). [c] Quasar photometry (R.A., Dec., $m_{\rm r}$) is from the Million Quasars Catalog (Flesch 2015, 2017). [d] Redshift from MAGGI (Lofthouse et al. 2020). [e] Redshift from NED.

Release Notes

Data Reduction and Calibration

The products included in this data release have been reduced using CubEx reduction software (Cantalupo et al. 2019 and in prep). This additional reduction performed using CubEx improves on the data products released in DR1 by correcting residual imperfections in the sky subtraction and illumination corrections as shown in Fig 1. of Lofthouse et al. (2020), and reproduced here.

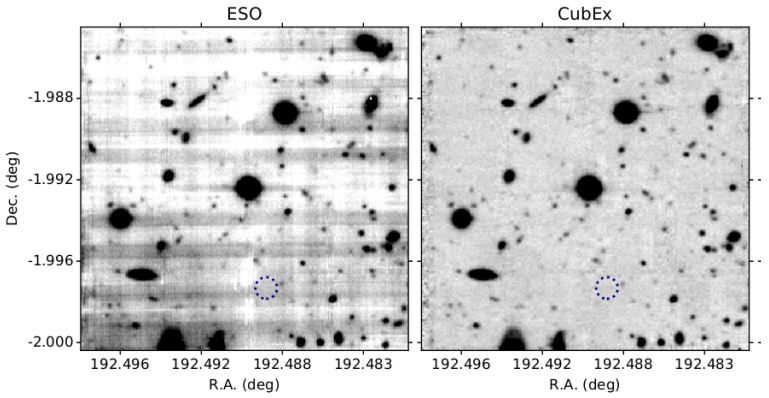

From Lofthouse et al. 2020, MNRAS, 491, 2057. doi:10.1093/mnras/stz3066

We begin with the standard reduction using the ESO pipeline. The reduction pipeline is based on the recipes distributed as part of the ESO MUSE pipeline (Weilbacher et al. 2014, version 2 or greater), which processes the raw data and applies standard calibrations to the science exposures. Briefly, the pipeline generates a master bias, a master flat, processes the arcs, and reduces the sky flats. Next, calibrations are applied to the standard star and a sensitivity function is then generated. Finally, these calibrations are applied to the raw science exposures and data cubes with associated pixel tables are reconstructed.

After this stage, we reconstruct cubes that are sky subtracted by the ESO pipeline with models of the sky continuum and sky lines that are computed using the darkest pixels in the field of view. After aligning the individual exposures by using point sources in the field, we generate a stack of all science frames into a single final cube. Finally, we register this final stack on a reference coordinate system by imposing an absolute zero-point for the world coordinate system using the position of the quasar at the centre of the field. For our reference system, we use Gaia astrometry (Gaia Collaboration 2018). Wavelengths are in air with barycentric corrections applied. Readers can refer to Lofthouse et al. 2019 (doi:10.1093/mnras/stz3066) for further details on the reduction.

Following this, we post-process individual exposures using the tools distributed as part of CubEx (v1.8). Briefly, we use an initial pass of the CubeFix tool to correct residual differences in the relative illumination of the 24 MUSE IFUs and of individual slices followed by CubeSharp which implements an algorithm to perform local sky subtraction. This applies a more accurate removal of the sky lines compared to the standard ESO pipeline. These steps are applied iteratively to achieve the highest quality masking of sources within each of the datacubes. We combine all the individual exposures for each sightline into a single data cube, masking edges and visually inspecting each exposure to manually mask out any artefacts. From the resulting high S/N datacube, we create the white-light CubEx image. Readers can refer to Lofthouse et al. 2020 (doi:10.1093/mnras/stz3066) for further details on the reduction.

Data Quality

The CubEx reduction procedure is successful in improving the sky subtraction, especially for sky lines at $\lambda > 7000$Å and in the continuum at $\lambda < 5500$Å. To quantify the relative improvement with respect to the ESO reduction, we compute the ratio of the flux standard deviation in a sky

spectrum within the range 6000-9000Å, finding a ratio of 0.30 for the CubEx reduction compared to the standard ESO one.

Likewise, the CubEx reduction pipeline significantly improves the quality of the illumination homogeneity across different IFUs and slices. The uniformity of the illumination can be quantified by comparing the flux standard deviation of sky pixels in the white-light image from the CubEx processing relative to the ESO reduction. We find a ratio of 0.14 confirming the visual impression from Fig. 1 of Lofthouse et al. (2020).

The detector noise is propagated through the various reduction steps however due to the multiple transformations performed on the pixels, the resulting pipeline variance does not accurately represent the effective standard deviation of the voxels in the final data cube, see Fig.2 in Lofthouse et al. (2020) and reproduced below (left). To correct for this, we bootstrap the pixels in the individual exposures using the resampled cubes after the CubEx post-processing to reconstruct an estimate of the noise for the final mean, median, and half-exposure cubes. We then use the bootstrap estimates to derive a wavelength-dependant scaling coefficient that we then apply to the pipeline variance.
While this method yields a better estimate of the pixel rms, the resampling of individual pixels introduces correlations that result in an underestimate of the effective noise and hence produce an overestimate of the S/N of a source. To model the change in noise as a function of number of pixels within an aperture, we compute the effective noise σ_{eff} as the standard deviation of fluxes from empty regions (Fig. 3 of Lofthouse et al. (2020) and reproduced below (right)). A quadratic fit to the median ratios across the different cubes yields an expression of the form $\sigma_{eff}/\sigma_N = 1.429 + 0.091L - 0.008L^2$ where L is the diameter of the aperture in arcsec. This fitting function is useful to estimate the corrected S/N of extended sources.

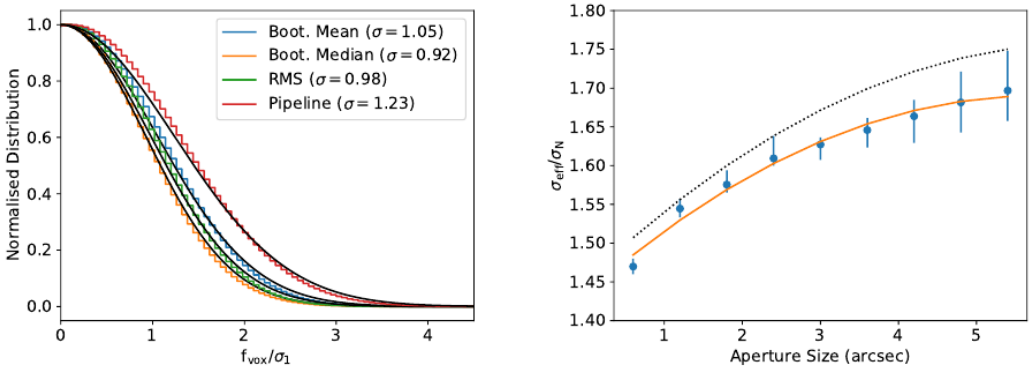

From Lofthouse et al. 2020, MNRAS, 491, 2057. doi:10.1093/mnras/stz3066

Previous releases

There is one previous data release from this project (DR1) which contains the 23 MUSE cubes observed as part of our large Programme ID 197.A-0384. These datacubes were reduced using the standard ESO reduction pipeline. In comparison, this release (DR2) contains the same 23 MUSE cubes along with an additional 5 from archival observations which have all been post-processed using the CubEx software.

Data Format

Files Types

The cubes and white-light images released follow the standard format described in the MUSE pipeline manual with the '_cubex' suffix to indicate reduction using the CubEx software. Cubes and images are named according to the following convention:
JHHMMSS.ss+DDMMSS.s_cube_cubex.fits
JHHMMSS.ss+DDMMSS.s_image_cubex.fits

where JHHMMSS.ss+DDMMSS.s is the short form of the quasar R.A. and Dec. (J2000).

Acknowledgements

Publications making use of these data should acknowledge the paper accompanying the data release of this programme: Lofthouse et al. 2020, doi: 10.1093/mnras/stz3066.

The data reduction has been completed while receiving funding from the European Research Council (ERC) under the European Union's Horizon 2020 research and innovation programme (grant agreement No 757535).

To access the codes and scripts used, please visit http://www.michelefumagalli.com/codes.html.

Any publication making use of these data, whether obtained from the ESO archive or via third parties, must include the following acknowledgment:

- "Based on data products created from observations collected at the European Organisation for Astronomical Research in the Southern Hemisphere under ESO programme 197.A-0384 "

If the access to the ESO Science Archive Facility services was helpful for you research, please include the following acknowledgment:

- "This research has made use of the services of the ESO Science Archive Facility."